AD-A099 158 ILLINOIS UNIV AT URBANA DEPT OF METALLURGY AND MINING--ETC F/G 11/6
THE EFFECT OF HYDROGEN ON THE FRACTURE AND SLIP BEHAVIOR OF NIC--ETC(U)
MAR 81 F HEUBAUM, H K BIRNBAUM N00014-75-C-1012
UNCLASSIFIED NL

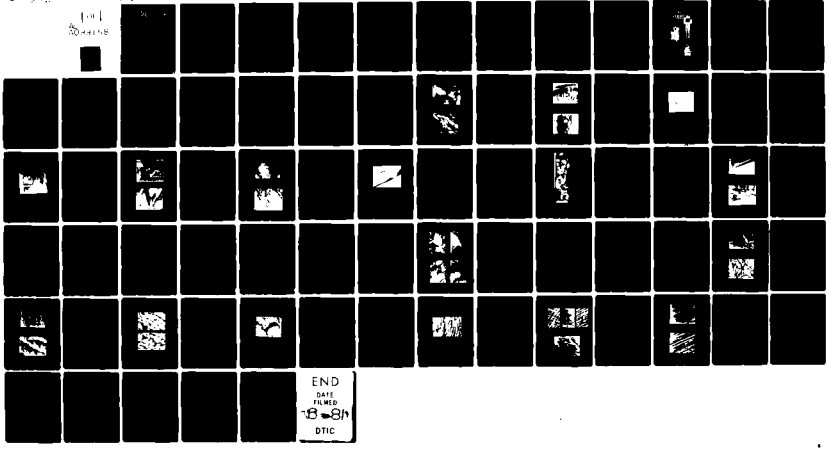

END
DATE FILMED
6-81
DTIC

LEVEL I (1) 20

THE EFFECT OF HYDROGEN ON THE FRACTURE AND SLIP BEHAVIOR OF NICKEL

(10) FRANK HEUBAUM AND H. K. BIRNBAUM

University of Illinois at Urbana Champaign
Department of Metallurgy and Mining Engineering
Urbana, IL 61801

(9) Technical Report-3-1 Office of Naval Research

(12) Contract USN N00014-75-C-1012

(11) March 1981

TABLE OF CONTENTS

1. INTRODUCTION

The tensile behavior and fracture of nickel single and polycrystals in the presence of hydrogen has been studied by several investigators in the past two decades.[1-5] It has been previously shown that hydrogen, whether introduced cathodically, thermally or from a gaseous atmosphere, causes the fracture mode of nickel polycrystals to change from a ductile microvoid coalescence with severe necking to a primarily intergranular separation.[5-8] Intergranular cracks nucleate preferentially at grain boundary triple points and grow by grain boundary shearing. Several triple point cracks may open at different regions across the gage length. These secondary cracks may later link together and join the main crack as straining continues.

In this experiment a low temperature tensile stage was built for a JEOL JSM-35C scanning electron microscope in order that the mechanisms of such cracking could be studied in situ. Video tape recordings were also made of the fracture process. A similar system was built by Grossbeck[9] in a study of hydrogen embrittled bcc niobium.

As in bcc materials, the degree of embrittlement of thermally charged polycrystals of nickel was found to be sensitive to temperature and strain rate variations.[10] The ductility as measured by reduction in area has a minimum at approximately -80°C with smaller secondary minima at -120 and 20°C. The ductility minimum at -80°C corresponds to the temperature region where serrated yielding is most pronounced. Here the hydrogen diffusion rate and the dislocation velocities are comparable, resulting in continuous pinning and depinning of dislocations.[11] A decreasing strain rate similarly decreases fracture ductility. The strain rate effect is most prominent at

temperatures high enough to allow appreciable hydrogen diffusion.[12] Another important factor is the actual amount of hydrogen dissolved in the specimen. The effect of hydrogen is to minimize the reduction in area at fracture to about 20% at concentrations above 0.05 atomic percent hydrogen. Reduction in area increases rapidly below 0.03% H. Thus, it is important to keep specimens at low temperatures prior to testing in order to prevent significant loss of hydrogen. The solubility of hydrogen is given by the expression:

$$S = p^{1/2}\Phi / D$$

where S is the solubility in cc H_2 per cc Ni at STP , Φ is the permeability of hydrogen in nickel = 2.3×10^{-2} exp(-13090/RT) $cm^3/cm\text{-}sec\text{-}atm^{1/2}$, and D is the diffusivity of hydrogen in nickel = 4.02×10^{-3} exp(-9390/RT) cm^2/sec.[13]

Nickel single crystals fail by ductile shear when strained in vacuum or in an inert atmosphere whether they are thermally hydrogen charged or not.[14] However they have been found to fail by transgranular cleavage when the specimens are sharply notched and strained in an atmosphere of hydrogen gas. Kamdar[7] reported this fracture plane to be of the {113} type while Lynch[15] stated it is the {100} since he found slip traces intersecting the fracture plane at right angles to each other. The present investigation, using two surface X-ray analysis, finds that the fracture plane actually parallels the slip planes as will be shown subsequently.

Transgranular fracture may also occur in large grained polycrystals when tested in gaseous hydrogen. The relative proportion of transgranular fracture to intergranular fracture was found to be dependent upon the presence of sulfur segregated to the grain boundaries and the location or angle of the grain boundary to the advancing crack. Matsumoto and Birnbaum[16] have used scanning Auger electron microscopy and Ion Probe

(SIMS) techniques on fracture surfaces to show an increasing propensity for intergranular cracking when sulfur was segregated to the grain boundaries. Sulfur segregation was achieved by annealing the specimens at 1173 K for one hour followed by slow cooling, whereas a homogeneous distribution was obtained by annealing at 1573 K and rapidly cooling or quenching. In the absence of gaseous hydrogen the sulfur segregated specimens showed completely ductile behavior. Sulfur segregation experiments at higher sulfur levels without the influence of hydrogen have shown a decreased yield strength and fracture ductility as the cooling rate was decreased.[17, 18] A large amount of intergranular fracture was obtained in these experiments as well when large quantities of sulfur were segregated by slow cooling after an anneal at 875 K. In the presence of hydrogen, intergranular cracking may require less sulfur to be segregated.

Latanision and Opperhauser[19] have shown using Auger electron spectroscopy that other impurities segregated to grain boundaries enhance intergranular cracking during cathodic charging of hydrogen. In particular they found that Sb, Sn, and P act as recombination poisons that stimulate the adsorption of hydrogen in the metal preferentially at grain boundaries. In the present experiment neither Sb, Sn nor P were found on the intergranular fracture surfaces.

Several mechanisms for the observed embrittlement have been proposed[20] although no single one has been unquestionably accepted in the case of nickel. A list of these mechanisms is given below:

a) high pressure bubble formation
b) surface adsorption and decohesion
c) hydride precipitation
d) plastic deformation effects

The formation of high pressure gas bubbles or a film at grain boundaries is said to change the constraint conditions at microcracks for easier crack growth. It would not explain the observed crack nucleation at surfaces and the areas of nonmicrovoid transgranular cracking in hydrogen atmospheres. This proposal is now falling into disfavor. Surface adsorption and decohesion effects which would reduce the binding energy between Ni-Ni bonds at grain boundaries or at a transgranular crack tip were originally proposed by Troiano[21] and later by Oriani[22] for the case of steels. Direct evidence for this mechanism has not yet been adequately shown. In the case of Ni some doubt has been cast on the surface adsorption model by the work of Clark[23] using the method of zero creep to measure changes in surface energies at high temperature in hydrogen and in inert atmospheres.

Hydride precipitation is known to occur in nickel at high hydrogen pressures (greater than 10,000 atm.) or when using high current densities during cathodic charging.[1] On decomposition of the hydride, considerable grain boundary and transgranular cracking does occur. However at lower current densities or using thermal charging of hydrogen from low pressure H_2 atmospheres no hydride is known to form although intergranular cracking still occurs. Smith[24] reports seeing small triangular markings on some grain boundary fracture facets which he says may be due to the presence of hydride platelets.

Hydrogen embrittlement of Ni may also be due to plastic deformation effects by means of hydrogen enhancement of glide. Eastman[25] has recently shown that the flow stress of nickel polycrystals in H_2 gas is somewhat lower than in helium when pulled at very slow strain rates (10^{-7} sec^{-1}). Impurity concentrations such as C may have some influence on these results. In situ

straining experiments in a HVTEM have shown greater numbers of dislocations and higher mobility in H_2 gas than in vacuum.[25] Further evidence for this mechanism includes the observation of intense grain boundary shearing as seen in the video tape recordings done in this experiment, clear deformation markings even on intergranular surfaces, secondary cracking along deep slip bands, and transgranular fracture along (111) planes in H_2 gas atmospheres also shown in this investigation.

2. EXPERIMENTAL PROCEDURES

2.1 SEM Tensile Stage

A tensile cold stage shown in Figure 1 was constructed for use on a JEOL JSM-35C scanning electron microscope (SEM). The temperature of the stage could be controlled between room temperature and liquid nitrogen temperature. Temperature regulation was achieved by balancing the heat input of a 150 watt encapsulated quartz lamp to a dewar of liquid nitrogen connected to the stage with a braided copper strap. A thermocouple located near the quartz lamp was used with a temperature controller and the temperature of the specimen was monitored by a pair of thermocouples on the two specimen grips.

Straining was accomplished by moving the grips with a threaded screw shaft. A stepping motor was used to rotate the shaft and allowed a variation of crosshead speeds between 1.0×10^{-6}mm/sec (4.2×10^{-8}in/sec) and 2.6×10^{-1}mm/sec (1.0×10^{-2}in/sec). The stepping motor also allowed the crosshead to be stopped or reversed in order that the specimen may be unloaded to prevent further crack propagation while taking photographs of the crack front. Stress-strain curves were obtained by using a piezoelectric quartz washer to measure the load across the specimen as recorded on a strip chart recorder and strain was derived by using a pulse counter to the stepping motor to indicate the total elongation of the specimen. Video tape recordings were made of the entire fracture process. These could be replayed in slow motion if necessary to examine in detail the crack propagation and evolution of slip bands.

A 40 cm long chamber of the same diameter as the SEM specimen transfer

Figure 1. Cold stage for JSM-35C scanning electron microscope.

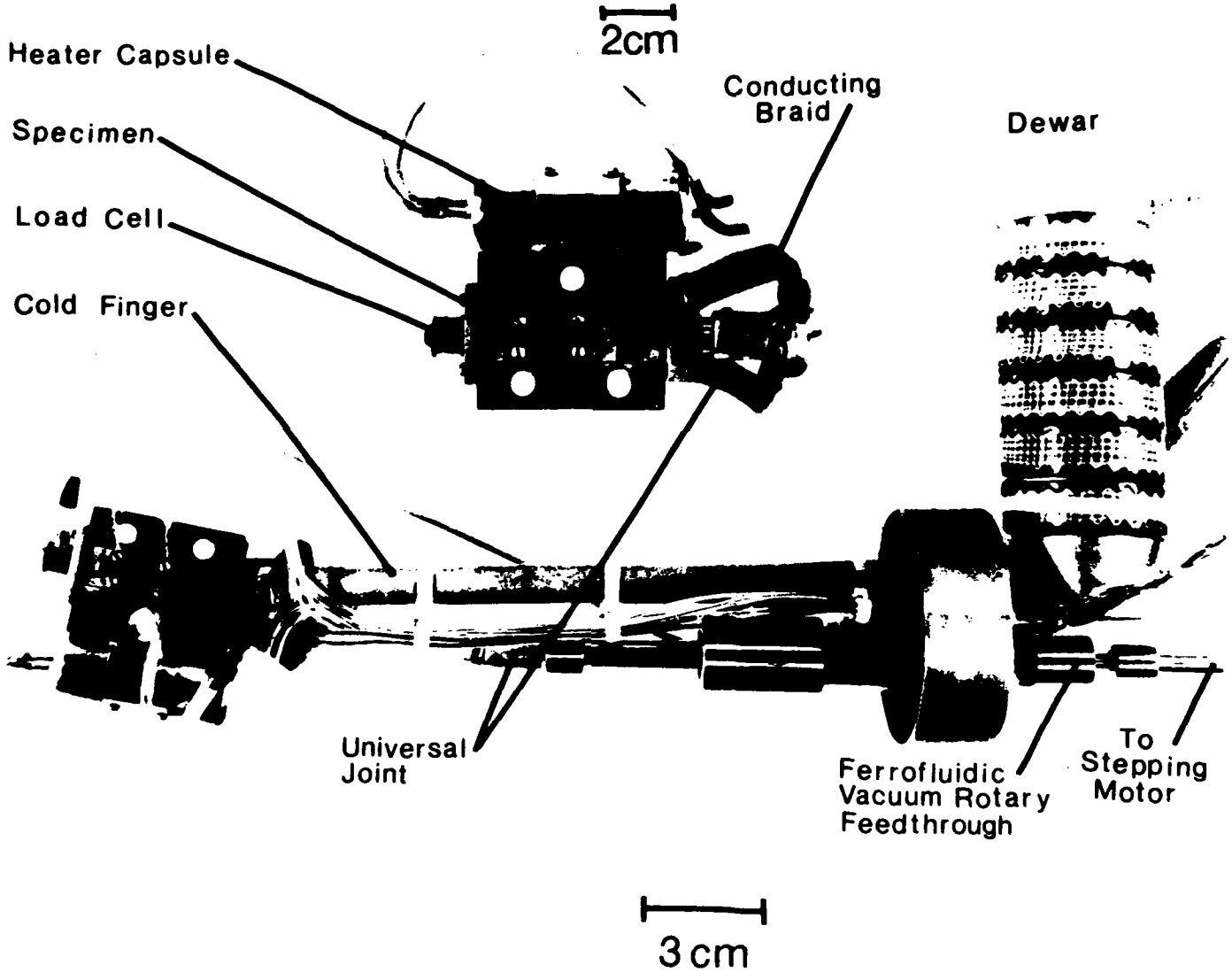
2cm
Heater Capsule
Specimen
Load Cell
Cold Finger
Conducting Braid
Dewar
Universal Joint
Ferrofluidic Vacuum Rotary Feedthrough
To Stepping Motor
3 cm

chamber opening and which could be evacuated and backfilled with hydrogen was constructed to allow tests to be conducted in a hydrogen atmosphere outside the microscope using the same tensile stage.

2.1.1 SEM Tensile Sample Preparation

Nickel tensile specimens whose dimensions are given in Figure 2 were machined from nominally one millimeter thick sheet. The chemical analysis for trace elements in this sheet is given in Table I. All specimens were first polished in a Buehler bakelite specimen mount using rough polishing with 400 and 600 grit silicon carbide paper followed by final polishing on nylon wheels with 1.0, 0.3 and 0.05 micron alumina. Specimens 1-13 were next induction heated to 1623 K in 95% N_2 - 5% H_2 gas for one hour which resulted in an average grain size of 0.3 - 0.5mm. A larger grain size (0.7-1.5mm) was produced in subsequent specimens by using the following technique:

1. Anneal at 1623 K for 3 minutes
2. Strain specimen 2%
3. Anneal at 1623 K for one hour

The 95% N_2 - 5% H_2 gas mixure was used because of its reducing characteristics with respect to oxygen while at the same time keeping hydrogen solubility less than 0.01%. Also the solubility of nitrogen in nickel is less than 0.002% in both the solid and liquid states and it forms no nitrides at these elevated temperatures.[26] Following these anneals a notch with 0.02mm (20 μ) root radius was cut in the reduced section of the specimens using electric discharge machining (EDM) with a razor blade as the electrode.

Hydrogen charging was performed by induction heating the specimens in flowing, dry hydrogen gas for 30 minutes at 1623 K followed by quenching

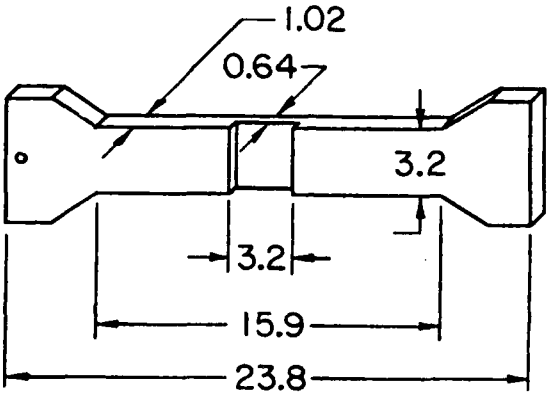

All dimensions in mm

Figure 2. Nickel tensile specimens

Table I

Analysis of Impurity Elements in
Nickel Tensile Specimens

Mass Spectrographic Analysis *	
Element	Concentration
Fe	10 appm
Ca	30
Co	1
Cr	≤ 3
Ti	≤ 1
Cl	1
Al	1
Mg	≤ 70
F	1
Vacuum Fusion Analysis	
C	3
O	0.4
S	none detected

* Mass spectroscopic analysis has an accuracy of ÷/× a factor of 3. All elements which are not listed are not present at levels above 1ppm.

$\leq$ Indicates the upper limit of concentration when evidence for its existence is inconclusive due to possible interference effects.

directly into 0°C silicone oil. The specimens were immediately stored in liquid nitrogen prior to testing to prevent outgassing of hydrogen. Several specimens were charged with hydrogen at 1073 K for one hour to allow sulfur to segregate to grain boundaries.

2.1.2 Scanning Auger Spectroscopy

One end of each specimen which had been fractured in the SEM or in H_2 gas was viewed in the SEM in order to characterize the fracture mode and to look at finer details on the fracture surface. The other end of selected specimens was placed in a scanning Auger electron spectrometer to determine the species of grain boundary segregates. Depth profiling was carried out across intergranular fracture facets by sputtering with 1.3 nA Xe ions. Using this procedure the proportion of S, Cl, and O to Ni was determined by monitoring the peak to peak heights of dN/dE of these impurities with respect to two Ni peaks as sputtering progressed.

2.2 Single Crystal Fracture Plane Determination

2.2.1 Sample Preparation

The 6.3 mm diameter single crystal Ni rod used in this part of the experiment was prepared using electron beam zone melting. A 4 cm long segment was cut from this rod and a pair of flat surfaces at exactly 90° to each other were planed lengthwise across the specimen using EDM. The specimen was mechanically polished as described for the SEM tensile specimens

with a final vibropolishing using 0.05 micron alumina to reduce the deformed surface layer. Back reflection X-ray Laue photographs were taken to determine the orientation of the flat faces and the crystal axis. A sharp notch was cut at the intersection of the two flat surfaces in the center of the crystal with a razor blade using the EDM unit.

2.2.2 Straining and Fracture Orientation of the Single Crystal

The crystal was fractured in an environmental chamber of a Tinius Olsen Locap Tensile Testing Machine which was designed to allow evacuation through a diffusion pump and then be backfilled with ultra high purity hydrogen gas. The specimen was pulled in tension in 2.8×10^4 Pa above atmospheric pressure (4 psig) H_2 gas at 298 K at a strain rate of 5.0×10^{-6} sec^{-1}. After fracture the angle which the fracture plane made with the flat surfaces was measured optically and in the SEM. These were then plotted on the stereographic projection made using the X-ray Laue patterns to determine the crystallographic fracture plane. SEM fractography was also performed on the transgranular fracture plane faces to characterize the type of fracture on a microscopic scale.

2.3 Slip Line Studies

The slip line appearance on the flat faces of the single crystal fractured in H_2 gas was studied in the SEM. Another single crystal segment prepared in a similar manner to the one described in Section 2.2.1 was strained to the same elongation in vacuum. The flat faces of this crystal were also viewed in

the SEM to compare the slip line structure.

A pair of 6.2 mm diameter polycrystalline rod specimens of the same composition as was given in Table I were prepared in the same manner as the single crystal specimens. These were then given a strain anneal cycle as described for the SEM samples to obtain a grain diameter of 1 - 3 mm. No notch was cut in these samples however. One specimen was pulled in hydrogen gas to 5%, 10%, 30% and fracture. The specimen was removed at each of these intervals for study in the SEM. The same procedure was used for the other sample which was strained in vacuum.

3. RESULTS AND DISCUSSION

3.1 Fracture Behavior in SEM Tensile Experiments

The specific testing conditions, specimen characteristics, and mode of failure of the nickel specimens used in this study are summarized in Table II. Specimens which were not exposed to hydrogen during the anneal or during the test failed by ductile microvoid coalescence with severe necking as shown in Figures 3 and 4. Following considerable uniform deformation across the entire specimen width, a ductile fracture initiates and the advancing crack (Fig. 3) exhibits a very large crack opening displacement (COD). At all temperatures between 123 K and 300K, 95% reduction in area (Fig. 4) was obtained. Yield stress and ultimate tensile stress were found to be 48 MPa (7000psi) and 250 MPa (36000 psi) respectively.

In sharp contrast to the previous behavior, specimens which had been thermally charged with hydrogen failed almost exclusively by intergranular separation as shown in Figures 5 and 6. Vacuum extraction analysis for hydrogen content in these charged specimens was performed which indicated a concentration of 700 atomic ppm solute hydrogen. An examination of the video tapes made during the fracture process showed that crack nucleation occurred at grain boundaries situated within the root of the notch or at grain boundary triple points ahead of the notch (Fig. 7). At least 10-15% plastic strain is undergone prior to crack nucleation. This is clearly seen in the form of deformation markings and slip lines on the surface grains, particularly near the notched region.

Table II

Testing Variables and Fracture Characteristics
of SEM Tensile Specimens

Specimen #	Testing Temperature °K	Strain Rate sec^{-1}	Hydrogen Introduction Mode	Reduction in Area %	Failure Mode
2	298	2.0×10^{-4}	Uncharged	95	100% MV
3	123	2.0×10^{-4}	Uncharged	95	100% MV
6	223	4.0×10^{-4}	H_2 Charged 1623 °K Strained in Vacuum (SEM)	--	95% IG 5% MV
7	193	2.0×10^{-4}		25	100% IG
8	193	4.2×10^{-5}		20	100% IG
9	123	3.5×10^{-6}		20	100% IG
10	193	2.1×10^{-5}		20	100% IG
11	298	2.0×10^{-4}	H_2 charged 1073 K Vacuum Strain	28	90% IG 10% MV
13	298	2.1×10^{-5}	Uncharged Strain in H_2 gas	85	10% TG 90% MV
14	298	2.0×10^{-4}	H_2 charged 1623 K Strain in H_2 gas	30	95% IG 5% TG
15	183	2.0×10^{-4}	H_2 charged 1073 K Vacuum Strain	30 95	95%IG 100% 5%MV MV
17	113	2.2×10^{-3}	H_2 Charged 1623 °K Vacuum Strained in SEM	35	90% IG 10% MV
18	223	2.2×10^{-3}		25	90% IG 10% MV
20	298	2.0×10^{-4}		30	90% IG 10% MV
21	298	2.0×10^{-4}		28	90% IG 10% MV
22	193	4.2×10^{-5}	H_2 charged 1073 K Strain in Vacuum	25	95% IG 5% MV

IG - Intergranular Failure
TG - Transgranular
MV - Microvoid Coalescence

Figure 3. Propagating microvoid type crack in an uncharged nickel specimen with severe surface deformation visable.

Specimen #3

Figure 4. SEM fractograph of microvoid failure in an uncharged nickel specimen.

Specimen #3

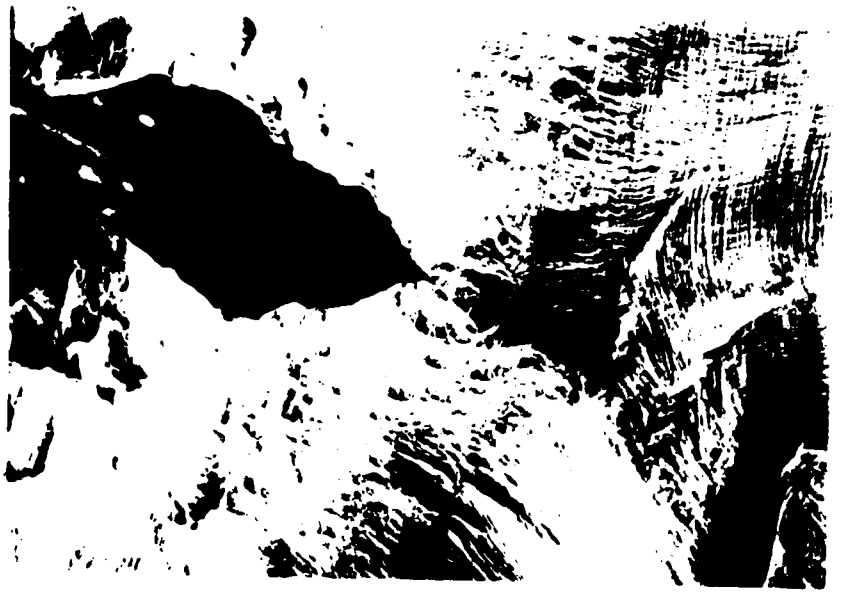

50μ

50μ

Figure 5. Intergranular failure in hydrogen charged specimen strained at 123 °K.

Specimen #9

Figure 6. Fracture surface of a hydrogen charged specimen showing nearly 100% intergranular fracture.

Specimen #9

250 μ

200 μ

Figure 7. An intergranular crack nucleated at a triple point ahead of the notched area.

Specimen #8

20 μ

A crack, once nucleated, will continue to propagate rapidly along the grain boundary until it encounters an unfavorably oriented grain at the next triple point. A large amount of localized shear would then occur along the grain boundary of the opposing grain thereby enlarging the COD as shown in Figure 8. During this process other secondary cracks may nucleate ahead of the main crack at grain boundaries and especially at triple points as illustrated in Figures 9 and 10. These secondary cracks may later link together as straining continues. This type of fracture occurs even at 113 K where the hydrogen diffusion rate is too slow to allow hydrogen to diffuse to the rapidly advancing crack tip. The relatively large COD and macroscopic ductility (25% R.A.) indicate that the fracture of hydrogenated nickel is not truly a brittle process but involves significant plasticity. Examination of the fracture surface further supports this fact in that although the fracture may approach 100% intergranular, the grain boundary fracture facets are rarely completely featureless as would be expected if fracture were due to a true decohesion process. Figure 11 shows an intergranular fracture surface which clearly reveals the deformation accompanying failure in the form of well defined intersecting slip lines. A few specimens also showed distinct cracking along slip lines on intergranular fracture facets (Fig. 12).

The effect of hydrogen on the failure mode can be completely eliminated by allowing the hydrogen to outgas from the specimen. This was shown using specimen #15 by straining the precharged sample until intergranular fracture had propagated half way through the specimen. The motor was then stopped and the temperature was raised from 183 K to 323 K and held there for 30 minutes. After recooling to 183 K straining was resumed and the fracture mode became ductile microvoid coalescence (Fig. 13) similar to uncharged specimens.

Figure 8. Intergranular fracture showing intense shear along a grain boundary resulting in a large COD.

Specimen #10

300 μ

Figure 9. Intergranular cracking in a charged specimen pulled at room temperature showing nucleation of secondary cracks ahead of the main crack and large COD.

Specimen #11

Figure 10. Intergranular cracking in a specimen pulled at 123 K showing secondary cracking and slip zone ahead of the crack.

Specimen #9


15KV X110
150μ


10KV X160 0905 100.0U M*F
100 μ

Figure 11. Intergranular fracture facets showing intersecting slip lines and ductility at an internal triple point.

Specimen #14.

Figure 12. Cracking along slip lines on an intergranular fracture surface.

Specimen #15

20 μ

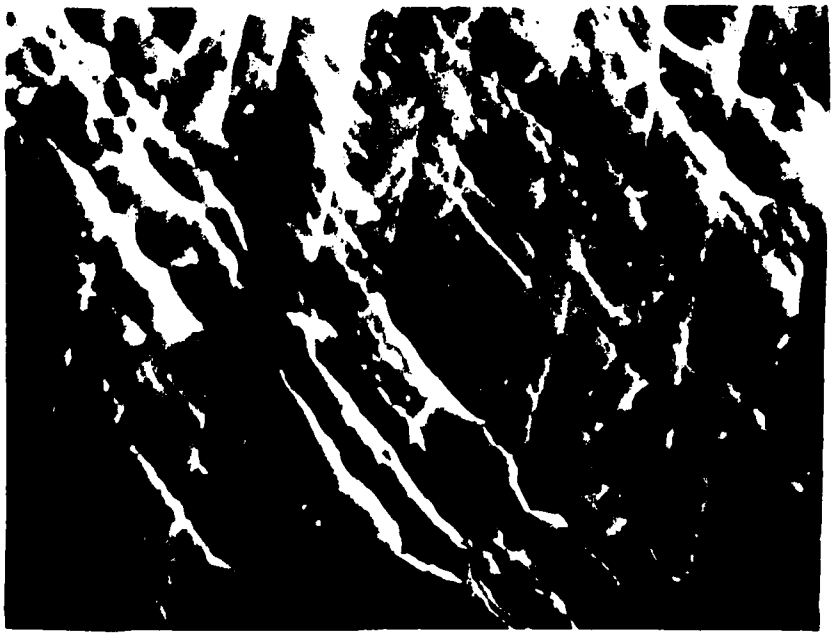

4 μ

Figure 13. Abrupt change in fracture mode from intergranular to ductile microvoid coalescence after depleting the hydrogen concentration.

Specimen # 15

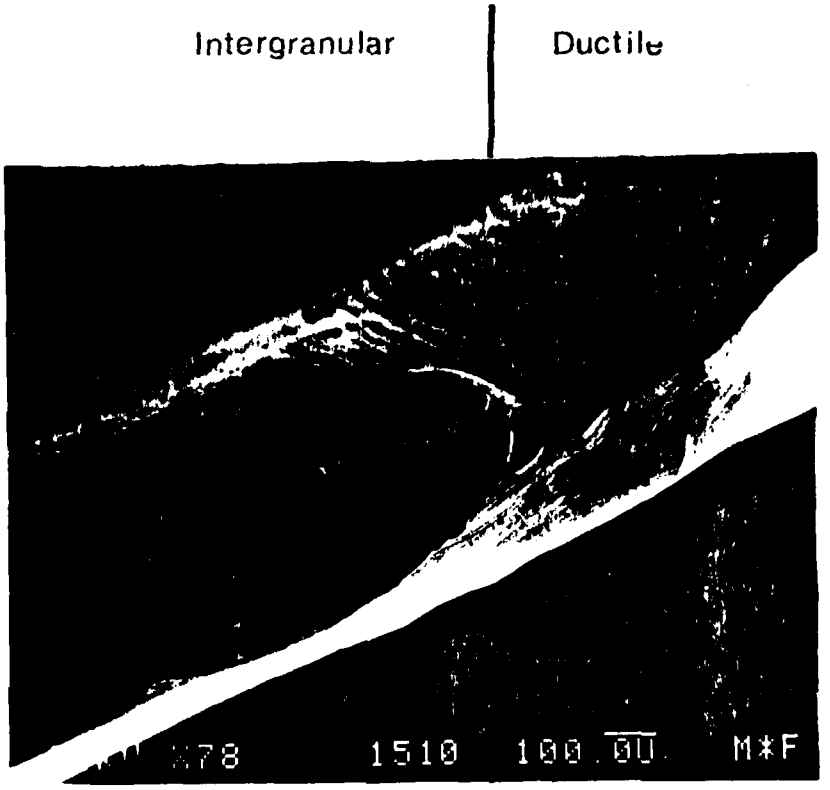

150 μ

The proportion of intergranular fracture to ductile microvoid type failure in thermally charged specimens was found to be sensitive to temperature, strain rate, and hydrogen content. As listed in Table II, the higher strain rates and temperatures give a somewhat larger fraction of microvoid failure. Under these conditions, microvoid regions usually occur in distinct areas along intergranular fracture facets as shown in Figure 14. Reduction in area is similarly affected by these variables as was demonstrated by Smith[12] whose results are given in Figure 15. The ultimate tensile strength of specimens thermally charged with hydrogen was only slightly higher (37,000-39000 psi) than those uncharged at the same temperature of straining but total elongation decreased from 60% to less than 20% at the minimum of ductility.

When well annealed, notched, nickel specimens which have not been thermally charged with hydrogen are strained in gaseous hydrogen, the fracture surface acquires distinct regions of transgranular fracture as shown in Figures 16 and 17. Note the extremely large COD and the slip markings along the sides and at the crack tip in Figure 16. The fractography will be discussed in more detail in the following section on fracture plane determination. If a grain boundary is properly oriented in the fracture path, regions of intergranular failure will also occur. This indicates that the energy difference between the two fracture modes is rather small in hydrogen atmospheres. The ductility of specimens showing predominantly transgranular failure is significantly greater than those with only intergranular fracture.

As was shown by Matsumoto and Birnbaum[16], the relative proportion of intergranular fracture to transgranular was dependent upon the concentration of sulfur at the grain boundaries. Using Auger electron spectroscopy, they

Figure 14. Fracture surface of a hydrogen charged specimen strained at room temperature showing distinct regions of microvoid failure.

Specimen #11


150μ

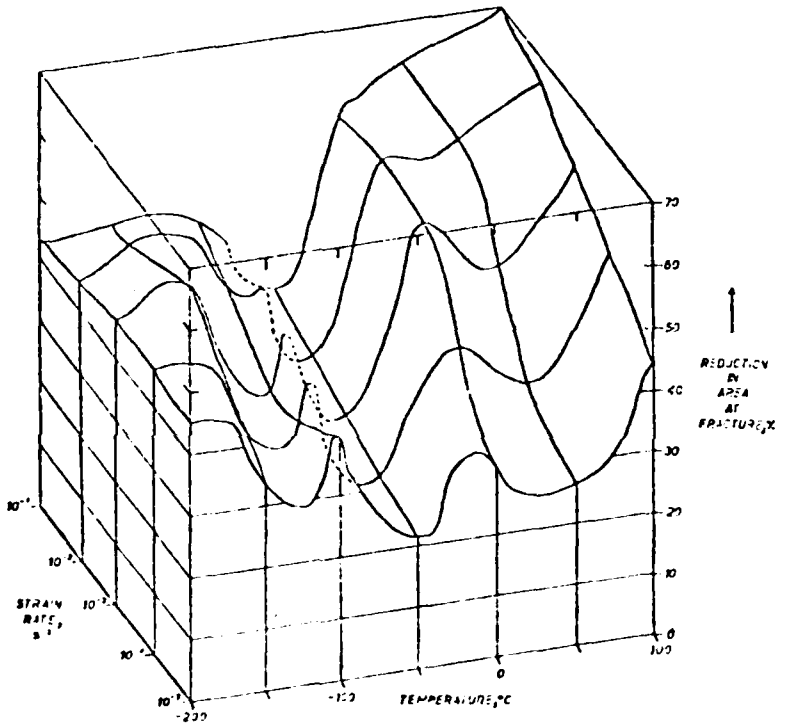

Figure 15. Reduction in area as a function of strain rate and testing temperature in hydrogen charged nickel specimens. After Smith (12).

Figure 16. A transgranular crack in a specimen pulled in H_2 gas showing the very large COD and slip lines along the crack especially at the crack front. Note also the areas of secondary cracking.

Figure 17. Fracture surface of a transgranular crack showing surface features and large reduction in area.

100μ

100μ

concluded that when nickel specimens are rapidly quenched from 1573 K, no sulfur segregation occurred and the resulting fracture was 80% transgranular when strained in gaseous H_2. However when slow cooled at a rate of 0.03 K/sec from 1173 K, sulfur segregation was found at the grain boundaries and as much as 80% intergranular fracture was obtained. Similar results were found in the present study. Auger electron spectroscopy and depth profiling were also carried out on the intergranular fracture surfaces of the thermally charged specimens described earlier. No sulfur segregation was found at the grain boundaries of specimens charged at 1623 K which indicates that in the presence of solute hydrogen, no sulfur need be present at the grain boundaries in order to promote intergranular fracture. Similarly no significant segregation of any other elements was found. A typical Auger signal and depth profile across the fracture surface are shown in Figures 18 and 19. The depth profile shows that as sputtering begins at time zero the surface contaminants O, Cl, and C begin to decrease as the Ni peaks increase. These contaminants are picked up primarily during handling after fracture and during specimen storage. The sulfur signal remains fairly constant at a relatively low level throughout the sputtering process.

When sulfur was purposely segregated to the grain boundaries by using a 1073 K anneal in H_2 gas, the fracture mode remained primarily intergranular. The Auger signal before and after sputtering with 1.3 nA Xe ions is shown in Figures 20 and 21. The sulfur peak is considerably reduced after sputtering and the depth profile (Figure 22) illustrates the higher concentration of sulfur at the grain boundaries. Again the surface contaminants mask the Ni and S peaks to a small extent prior to and during the onset of sputtering and account for the initial rise in the S peak. Fractographic studies in

Figure 18. Auger electron spectroscopy signal of a specimen annealed at 1623 K without sulfur segregation. The sulfur peak is barely visable in such specimens.

Specimen #8

Figure 19. Depth profile during sputtering with 1.3 nA Xe ions of the same specimen showing very little change in the concentration of sulfur as sputtering procedes through the grain boundary fracture surface. Only the level of surface contaminants is decreased.

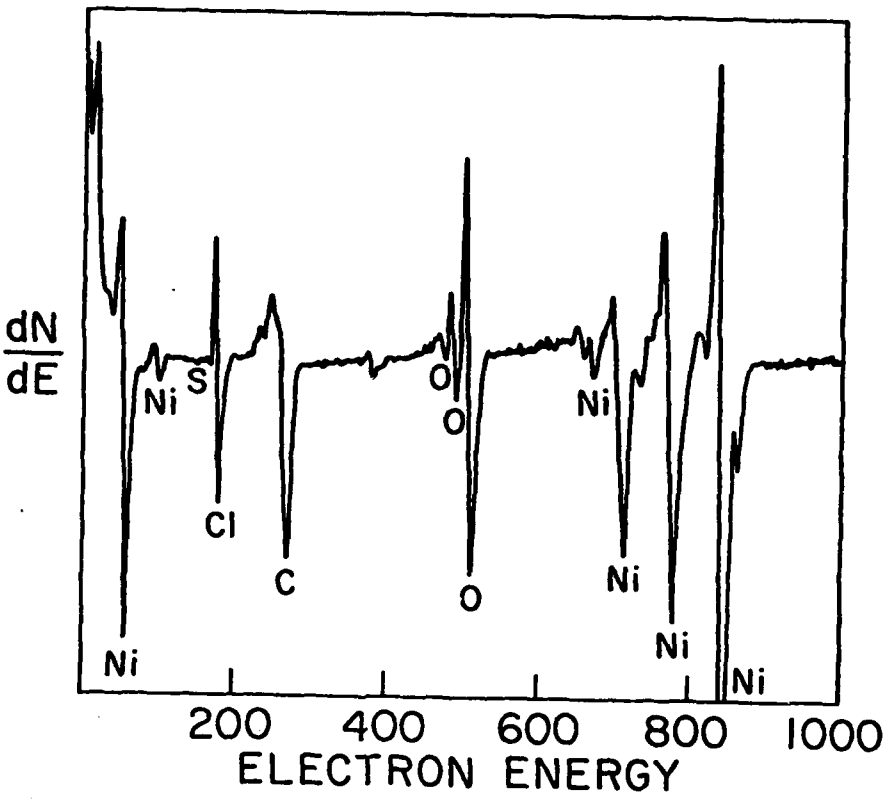
dN/dE
Ni
Ni
S
Cl
C
O
O
O
Ni
Ni
Ni
Ni
200
400
600
800
1000
ELECTRON ENERGY

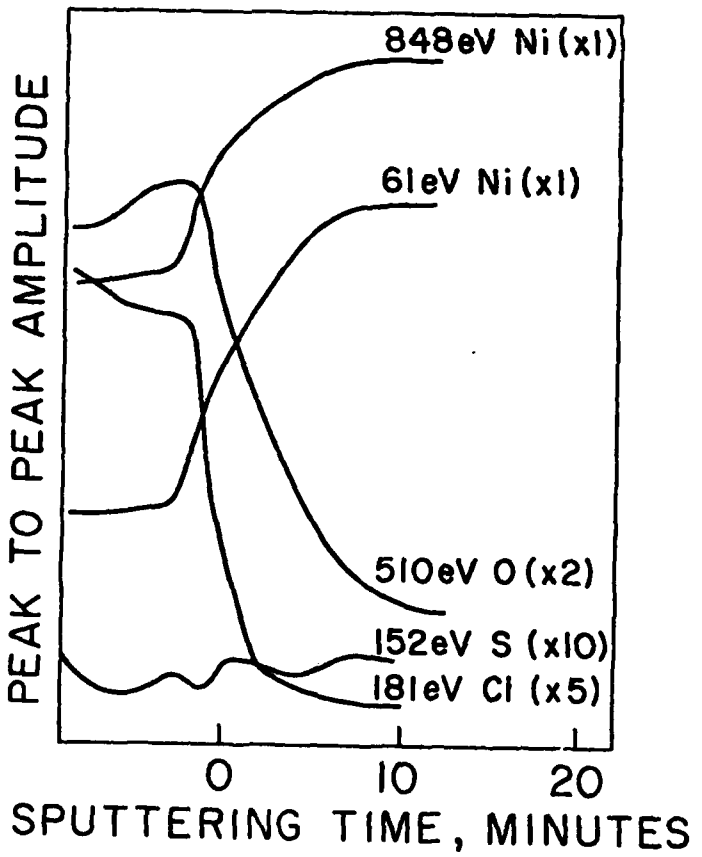
848eV Ni (x1)
61eV Ni (x1)
510eV O (x2)
152eV S (x10)
181eV Cl (x5)
PEAK TO PEAK AMPLITUDE
0
10
20
SPUTTERING TIME, MINUTES

Figure 20. Auger signal before sputtering of a specimen in which sulfur was segregated to the grain boundaries. The sulfur peak at 152 eV is much higher than was the case in Figure 18.

Specimen # 11

Figure 21. Auger signal after sputtering of specimen #11 showing the decrease in sulfur slightly beneath the grain boundary fracture surface.

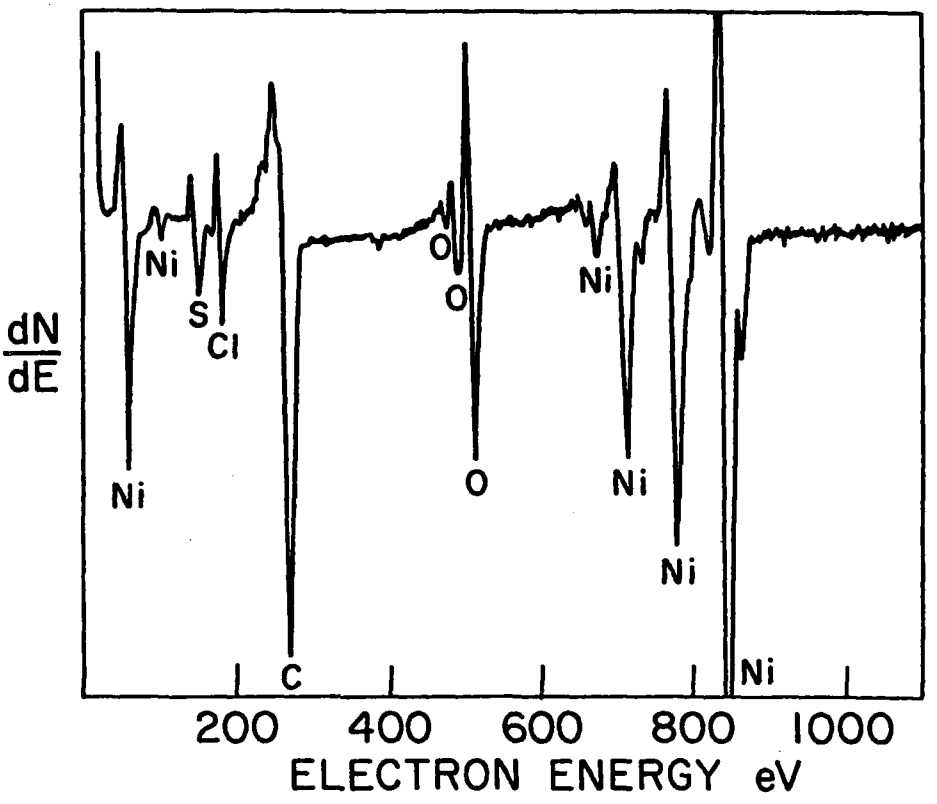
dN/dE
Ni
S
Cl
Ni
C
O
O
Ni
O
Ni
Ni
Ni
200
400
600
800
1000
ELECTRON ENERGY eV

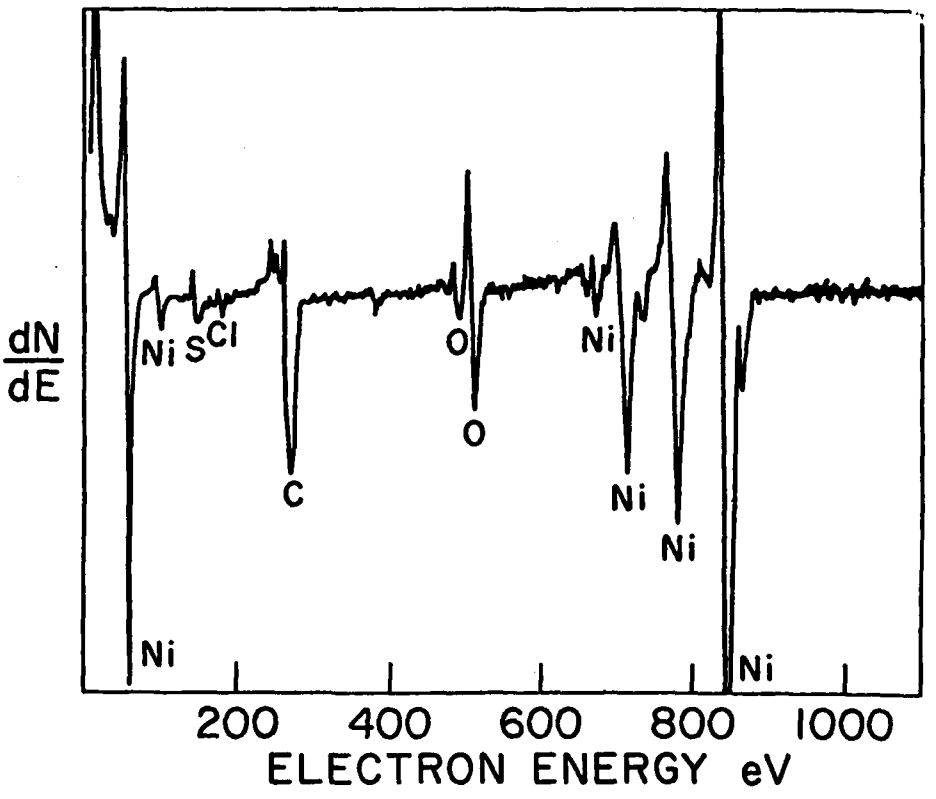
dN/dE
Ni
S
Cl
C
O
O
Ni
Ni
Ni
Ni
Ni
200
400
600
800
1000
ELECTRON ENERGY eV

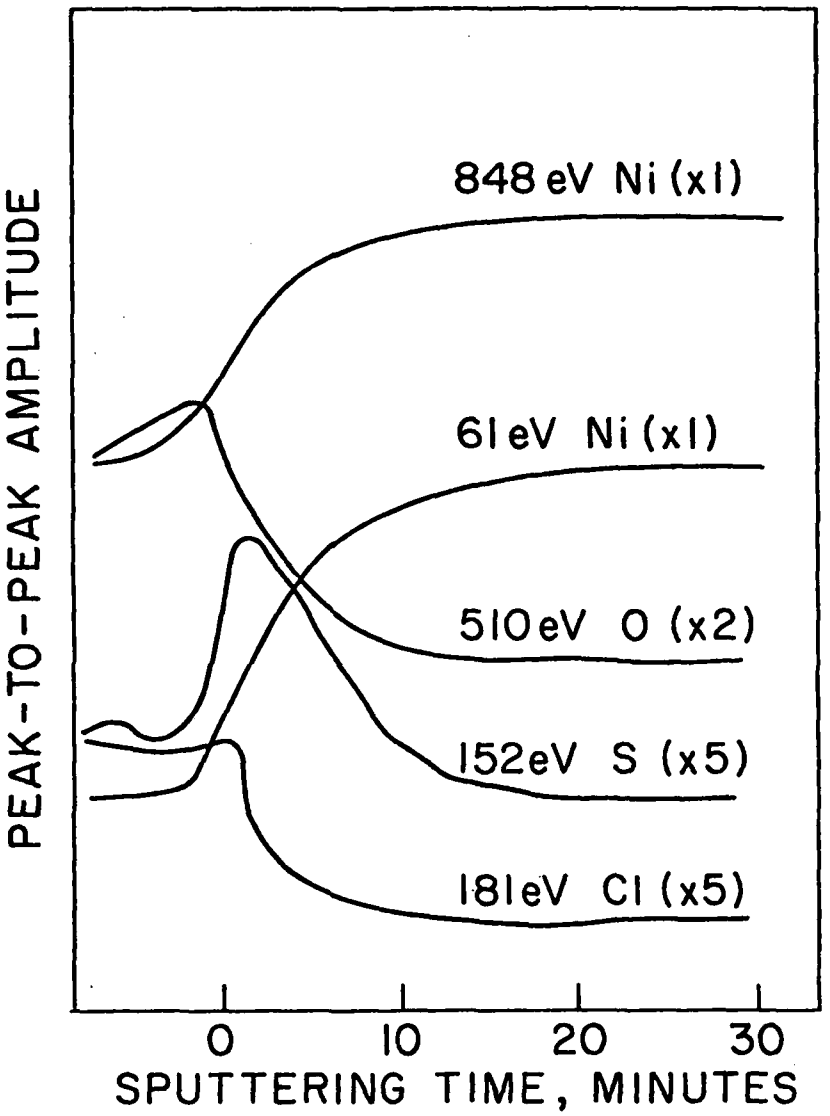

Figure 22. Depth profile during sputtering of specimen #11 shows the higher sulfur concentration at the grain boundary as seen by the diminisning amplitude of the sulfur signal as sputtering progresses deeper through the boundary.

the SEM indicated no evident differences in the transgranular fracture appearance between hydrogen charged specimens having sulfur segregation at the grain boundaries and those annealed at a higher temperature without segregation. This can be seen using the comparison illustrated in Figures 23 and 24 which are micrographs of a specimen without segregation and one with sulfur segregation respectively shown at two different magnifications.

In order to determine whether the intergranular fracture mode of specimens thermally charged with hydrogen or the transgranular mode of specimens pulled in hydrogen gas is the dominant mode, the following experiment was performed. A large grained, notched specimen was thermally charged with hydrogen at 1623 K. It was then strained to failure in a hydrogen atmosphere at 298 K similar to specimens which failed predominantly in a transgranular mode in the absence of solute hydrogen. The resulting fracture was almost totally intergranular indicating that solute hydrogen is the primary controlling factor in the fracture process. Small grained specimens fail intergranularly when thermally hydrogen charged but uncharged specimens strained in hydrogen gas fail primarily by ductile microvoid failure since the higher fracture stress induces more plastic relaxation instead of crack nucleation.

3.2 Single Crystal Fracture Plane Determination and Fractography

Unnotched nickel single crystals have been shown to fail by ductile shear in vacuum, nitrogen, or hydrogen gas. However in the presence of a sharp notch these crystals, when pulled in dry hydrogen gas, exhibit a transcrystalline quasi-cleavage type failure. A two surface X-ray analysis

Figure 23. Micrographs at two different magnifications of an intergranular fracture surface without sulfur segregation.

Specimen #8

Figure 24. Micrographs of an intergranular fracture surface of a specimen with sulfur segregation which had been fractured at the same temperature and strain rate.

Specimen #22

50 μ

10 μ

50 μ

10 μ

was undertaken to determine the crystallographic fracture plane in these crystals. The results are given in the stereographic projection in Figure 25. Fracture occurred along (111) slip planes inclined to the [221] specimen axis by 55°. Because these (111) planes are not very favorably oriented with respect to the tensile axis, the initial portion of the fracture surface shows a rather stepped appearance as illustrated in Figure 26. The steps correspond to parallel (111) planes. These observations contradict previous fracture plane reports of (100)[15] and (113)[7].

High resolution fractographic studies in the SEM revealed that the fracture is not truly a brittle cleavage process but involves significant local plasticity. Typical regions of the fracture surface appear as shown in Figures 27 and 28. The small tetrahedral hillocks and depressions seen in Figure 28 and at higher magnification in Figure 29 appear to have sides corresponding to intersecting (111) planes. (111) slip traces are also seen in these Figures parallel to the sides of the hillocks. An examination of opposite fracture surfaces reveals the geometry of how those tetrahedral hillocks mate. As shown in Figure 30 there is a point to point correspondence between hillocks on one side to those of the other. Points A-A* and B-B* are two of such corresponding points. This indicates that their formation is through a ductile necking type process. Further evidence for the (111) type fracture plane occurred in the form of a small void in the fracture path with (111) slip traces running circumferentially around it parallel to the fracture surface (Fig.31).

The micro-features described here for the case of single crystals are similar to those found in large grained polycrystals as was shown in Figure 17. Some indication of river lines are observed in the transgranular

Figure 25. Stereographic projection showing the orientation of the nickel single crystal and the fracture plane after straining in H_2 gas.

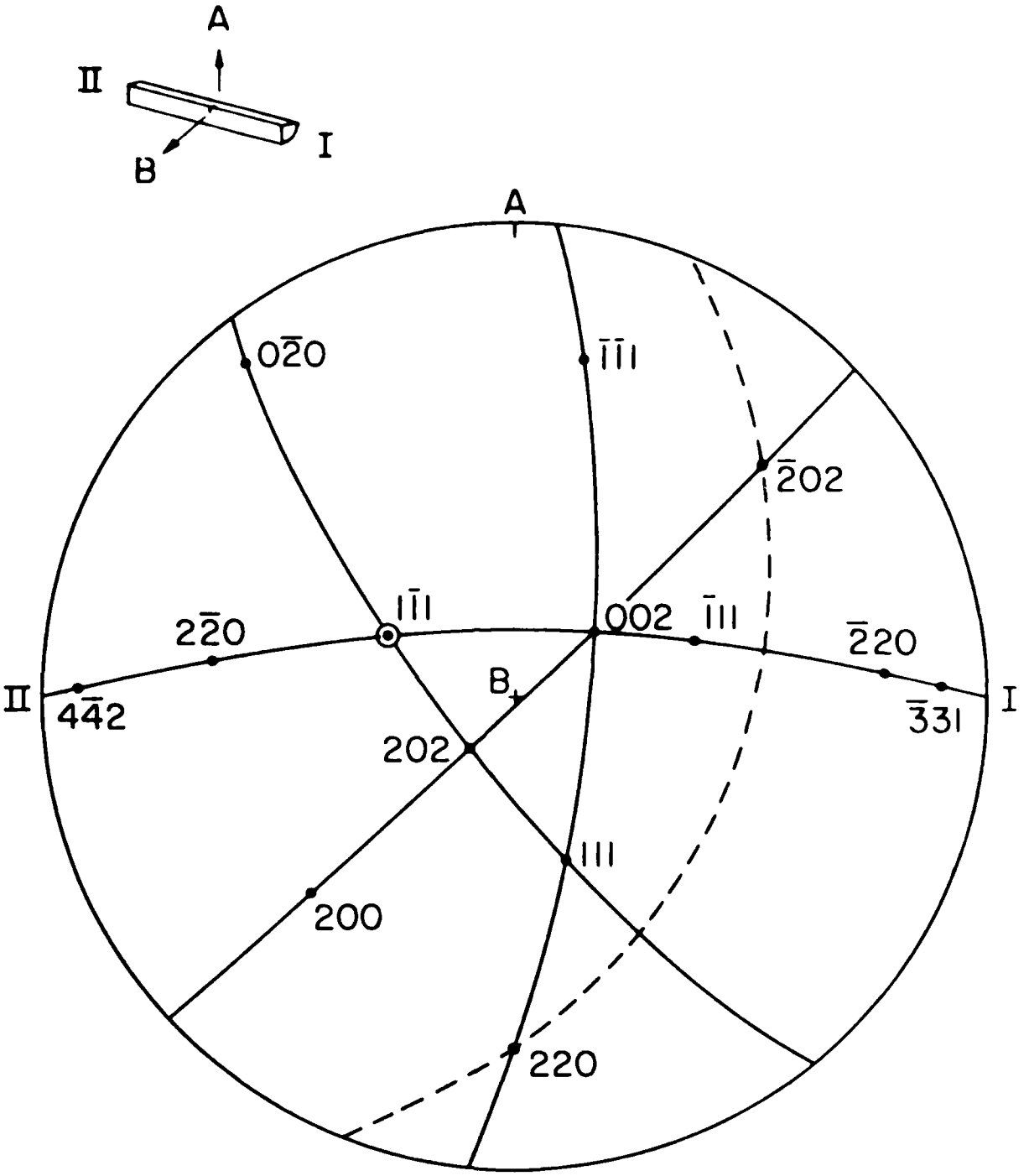

---- FRACTURE PLANE

⊙ NORMAL POLE TO FRACTURE PLANE

Figure 26. (111) fracture steps in single crystal fractured in H_2 gas.

Figure 27. Typical fracture surface features on single crystal.

200 μ

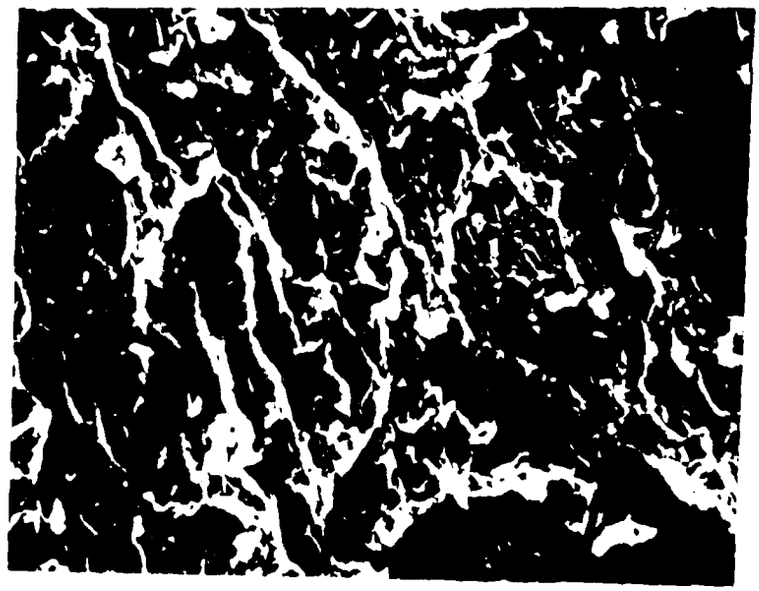

20 μ

Figure 28. Fracture surface features on (111) fracture plane showing hillocks and depressions along slip lines.

Figure 29. Higher magnification detail of hillocks on transgranular fracture plane.

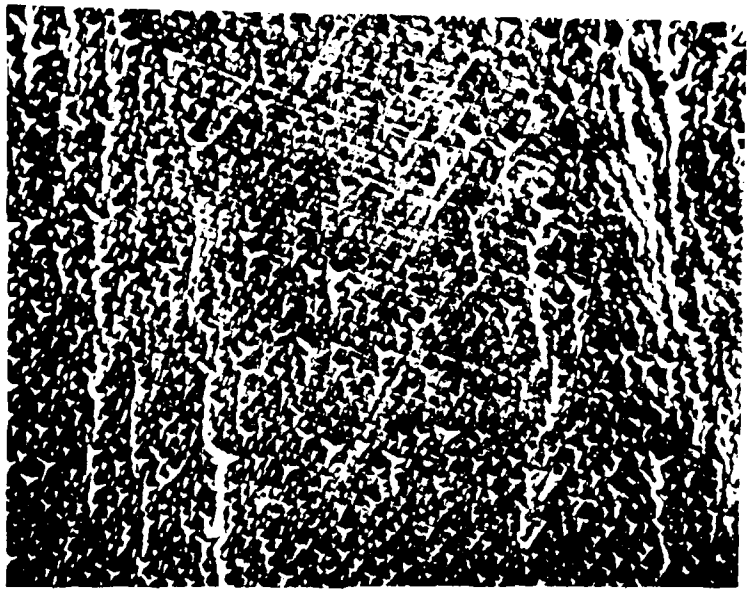

20 μ

3 μ

Figure 30. Opposite faces of the transgranular fracture plane showing the point to point correspondence between the hillocks on one side to those of the other. A - A* and B - B* are examples of the matching points.

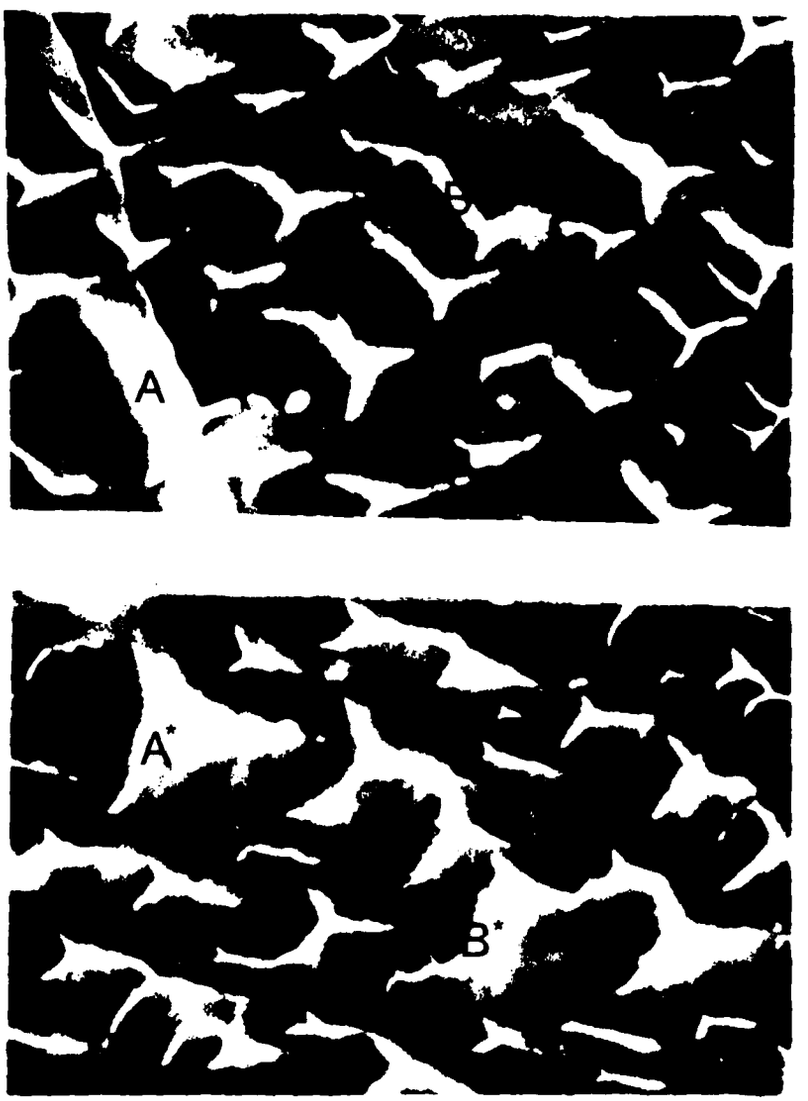
A
B
A'
B'
3 μ

Figure 31. A void in the fracture plane showing steps and slip lines circumferentially parallel to the fracture surface.

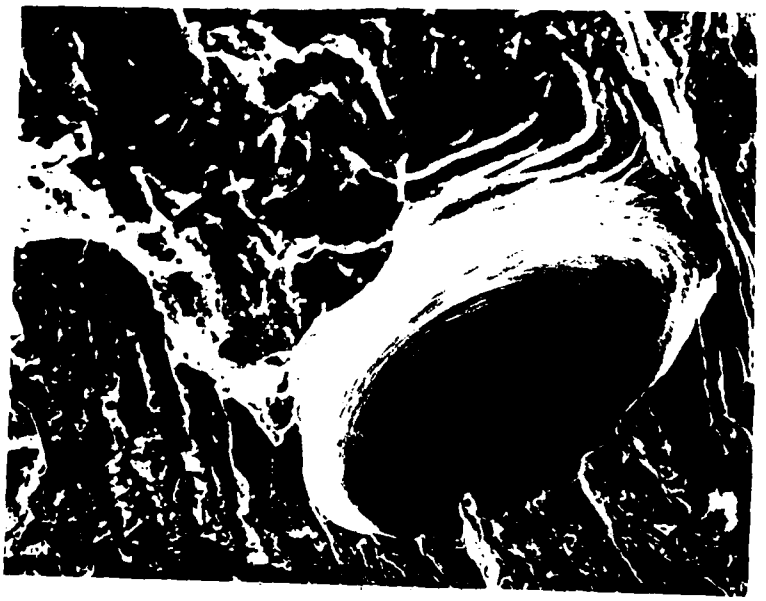

100 μ

fracture surfaces, but are less distinct than in purely brittle cleavage fractures. Secondary cracking is visible in many regions of these specimens as was seen in some of the previous micrographs and in Figure 32.

3.3 Effects of Hydrogen on Slip Line Structures

The single crystal used in the fracture plane determination had been strained to nearly 100% elongation at fracture. The two flat polished surfaces on this crystal showed very distinct slip characteristics. Surface (A) shown on the stereographic projection in Figure 25 contained clear secondary slip, the extent of which decreased slightly as the distance to the crack was increased as shown in the series presented in Figure 33. The other flat surface (B), 90° to the first, contained primarily single slip with considerable deformation banding as revealed in Figure 34. Another single crystal of the same orientation as the first was also strained to 100% but this time in vacuum. The flat polished faces of this crystal had undergone almost exclusively single slip as shown in Figures 35 and 36. The implications of these observations are not yet clear. Deformation banding is said to be most prominent in easy glide orientations where several slip systems are not operative throughout the crystal.[27] The crystal pulled in hydrogen showed both deformation banding and multiple slip on faces 90° to each other. The rounded part of the crystal also showed signs of deformation banding. Hydrogen in solution in Ni is reported to reduce SFE and thus decrease the amount of cross-slip.[12]

In order to examine the possibility that these effects were due solely to the special orientation of the crystals used, large grained polycrystals

Figure 32. Secondary cracking in the transgranular fracture plane.

10 μ

Figure 33. Multiple slip on a flat surface (A) of the single crystal fractured in hydrogen gas. The series shows the change in appearance as a function of distance to the crack.

Figure 34. Deformation bands on the other flat surface (B) of the single crystal.

Distance From Fracture

2mm

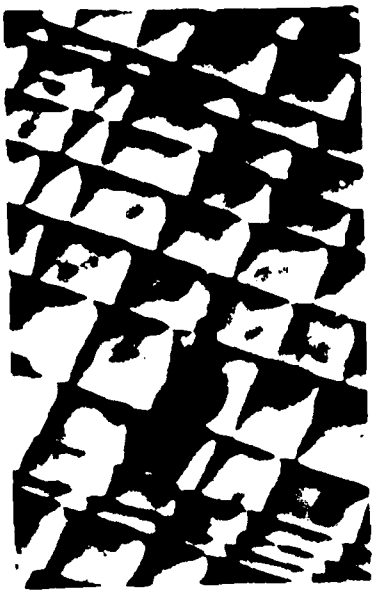

5 μ

5mm

10 μ

9mm

5 μ

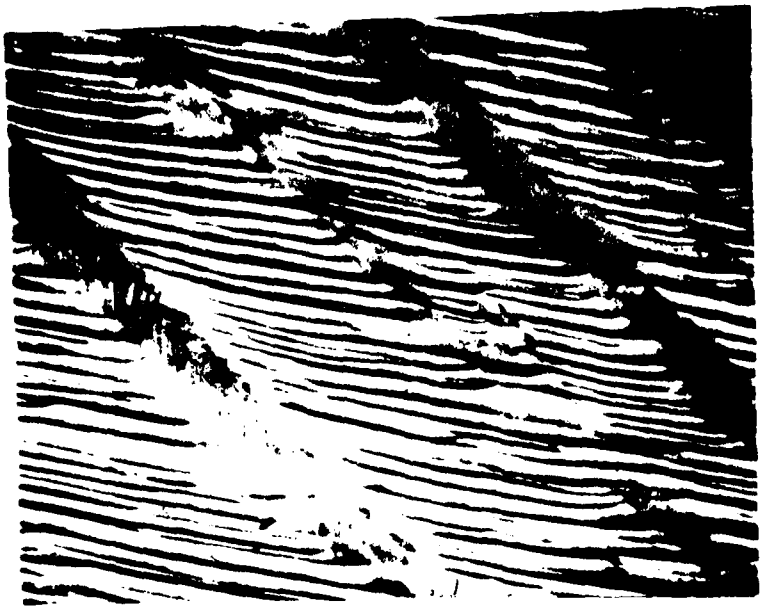

5 μ

Figure 35. Single slip on the flat surface of the single crystal strained in vacuum.

Figure 36. Higher magnification of slip lines shown in Figure 35.

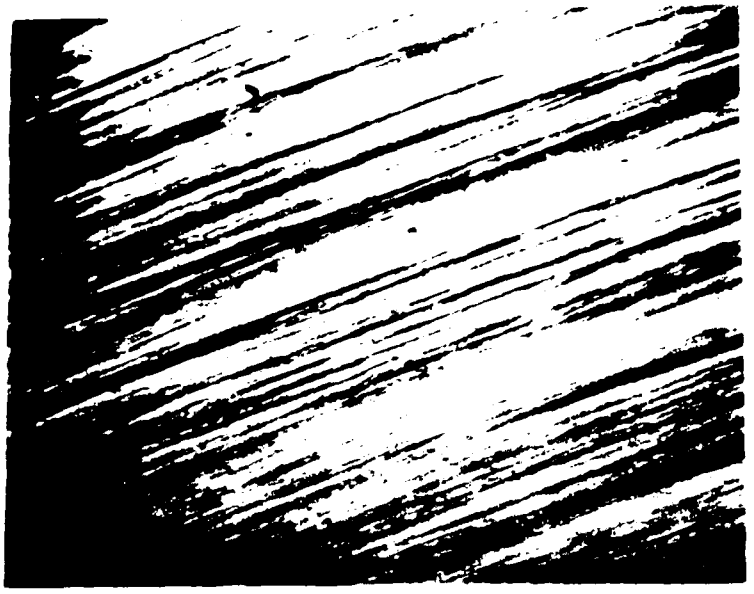

200 μ

2 μ

were prepared in a manner similar to the single crystals and strained 5%, 10%, 30% and to failure in H_2 gas and in vacuum. Slip line appearance varied between individual grains but no major differences were noticed between the specimens pulled in H_2 gas and in vacuum. McInteer, Thompson, and Bernstein[28] doing similar experiments using internally charged specimens, found an increase in surface slip planarity (decrease in slip line waviness) in hydrogenated specimens but little change in slip line spacing with strain.

3.4 Overall Implications of Results

The results, presented and discussed individually in the previous sections, include certain characteristics which are common throughout. Both intergranular and transgranular fracture processes are preceded by considerable plastic deformation prior to crack nucleation. Similarly, during crack growth, localized plastic processes occur at the crack tip under the influence of solute or gaseous hydrogen. These plastic processes manifest themselves in the form of intense grain boundary shearing which is clearly seen in the video tape recordings of the hydrogen charged specimens during fracture in the SEM. The formation of large COD's is an immediate consequence of this shearing as are the slip and deformation markings on the intergranular fracture facets.

During transgranular fracture in H_2 atmospheres, the plastic processes at the crack tip similarly result in an extremely large COD with the fracture surfaces showing slip traces and other features indicative of enhanced plasticity such as the tetrahedral hillocks formed by ductile necking. The transgranular fracture plane was found to be of the (111) type as determined by two surface X-ray analysis of nickel single crystals fractured in H_2 gas.

Failure along (111) planes, which are slip planes in fcc materials such as Ni, indicates that hydrogen at the crack tip locally interacts with dislocations on these planes and by increasing their mobility will lead to the plastic type of failure as observed.

The mechanism of enhanced plastic processes in hydrogen related failure of Ni briefly discussed here is consistent with the results obtained in in situ HVTEM studies in which upon the introduction of H_2 gas, dislocation generation and mobility increased dramatically. The lowering of flow stress in specimens tested in H_2 gas at strain rates of the order of 10^{-7} sec^{-1} is also an indication of the model's validity.

4. CONCLUSIONS

The introduction of hydrogen into nickel specimens by thermal charging leads to a predominantly intergranular failure mode regardless of sulfur segregation to grain boundaries. Following significant plastic deformation, crack nucleation occurs at grain boundary triple points and along grain boundaries situated within a stress concentration region. Large COD's are generated during crack growth through localized plastic deformation at the crack tip and intense grain boundary shearing. Grain boundary fracture facets show clear indications of such deformation in the form of slip with occasional cracking along slip lines. Secondary cracking at triple points ahead of the main crack is a common occurrence.

Transgranular fracture is observed in specimens having no significant sulfur segregation at grain boundaries when strained in H_2 gas. Two surface X-ray analysis in Ni single crystals show this fracture plane to be of the (111) type. This type of failure is also accompanied by considerable plastic deformation both prior to crack initiation and during crack growth. The fracture surface markings show evidence of this ductile failure with clear slip lines and tetrahedral hillocks whose faces appear to correspond to intersecting (111) planes.

The results presented in this thesis, along with previous work, indicate hydrogen related failure in nickel is due to a mechanism of hydrogen ennanced plastic processes at the intergranular or transgranular crack tips. In the case of transgranular failure, hydrogen enhances dislocation generation and increases their mobility along the (111) slip lines where eventual failure occurs.

REFERENCES

1. B. A. Wilcox and G. C. Smith, Acta Met. 12: 371 (1964).

2. M. R. Kamdar, ARC-10966, Ames Research Center, Moffett Field, CA. (October 1978).

3. M. R. Louthan, G. R. Caskey and J. A. Donovan, Paper presented at the Seventh Annual Technical Meeting of the International Metallographic Society, Gatlinburg, Tenn., (August 1974).

4. M. L. Wayman and G. C. Smith, Acta Met. 19: 227 (1971).

5. T. Boniszewski and G. C. Smith, Acta Met. 11: 165 (1964).

6. A. H. Windle and G. C. Smith, Met.Sci. J. 4: 136 (1970).

7. M. H. Kamdar, Paper 3D10 in Proceedings of the Second International Congress on Hydrogen in Metals, Pergamon, Oxford, (1977).

8. B. A. Wilcox and G.C. Smith, Acta Met. 13: 331 (1965).

9. M. L. Grossbeck, Ph.D. Thesis, University of Illinois, Urbana, (1975).

10. J. A. Snively, R. F. Hehemann and A. R. Troiano, Corrosion 23: 215 (1967).

11. R. M. Latanision and R. W. Staehle, Scripta Met. 2: 667 (1968).

12. G. C. Smith, in Hydrogen in Metals, I. M. Bernstein and A. W. Thompson, eds., ASM, Metals Park, pp. 485-511 (1974).

13. W. M. Robertson, Z. Metallkde. 64: 436 (1973).

14. A. H. Windle and G. C. Smith, Met Sci. J. 2: 187 (1968).

15. S. P. Lynch, Scripta Met. 13: 1051 (1979).

16. T. Matsumoto and H. K. Birnbaum, Hydrogen in Metals, Proceedings of the Second J. I. M. International Symposium, Transactions of the Japan Institute of Metals Supplement, 21: 493 (1980).

17. S. Floreen and J. H. Westbrook, Acta Met. 17: 1175 (1969).

18. K. M. Olsen, C. F. Larkin and P. H. Schmitt, Trans. ASM 53: 349 (1961).

19. R. M. Latanision and H. Oppernauser, Jr., Met. Trans. 5: 483 (1974).

20. H. K. Birnbaum, Environment - Sensitive Fracture of Engineering Materials, Z. A. Foroulis, ed., The Metallurgical Society of AIME, Warrendale, PA., p. 326 (1979).

21. E. A. Steigerwald, F. W. Schaller and A. R. Troiano, Trans. Met. Soc. AIME, 218: 832 (1960).

22. R. A. Oriani and P. H. Josephic, Acta Met. 11: 415 (1974).

23. E. A. Clark, R. Yeske and H. K. Birnbaum, Met. Trans. 11A: 1903 (1980).

24. M. L. Wayman and G. C. Smith, Acta Met. 19: 227 (1971).

25. J. Eastman, T. Matsumoto, N. Narita, F. Heubaum and H. K. Birnbaum, Paper presented in the Third International Conference on the Effect of Hydrogen on Behavior of Materials., August 1980, Jackson Lake Lodge, Moran, Wyoming., A. W. Thompson and I. M. Bernstein, eds. , New York, Metallurgical Society of AIME. (c. 1981).

26. R. P. Elliott, Constitution of Binary Alloys, First Supplement, McGraw-Hill, New York, p. 639,(1965).

27. R. W. K. Honeycombe, The Plastic Deformation of Metals, St. Martins Press, New York, p. 199, (1968).

28. W. A. McInteer, A. W. Thompson and I. M. Bernstein, Acta Met. 28: 887 (1980).

Unclassified

Security Classification

DOCUMENT CONTROL DATA - R & D

(Security classification of title, body of abstract and indexing annotation must be entered when the overall report is classified)

1 ORIGINATING ACTIVITY (Corporate author) University of Illinois at Urbana Champaign	2a. REPORT SECURITY CLASSIFICATION Unclassified 2b. GROUP

3 REPORT TITLE

The Effect of Hydrogen on the Fracture and Slip Behavior of Nickel

4 DESCRIPTIVE NOTES (Type of report and inclusive dates)

Technical Report

5 AUTHOR(S) (First name, middle initial, last name)

H. Frank Heubaum and H.K. Birnbaum

6 REPORT DATE	7a. TOTAL NO. OF PAGES	7b. NO. OF REFS
March 1981	69	28

8a. CONTRACT OR GRANT NO.	9a. ORIGINATOR'S REPORT NUMBER(S)
USN 00014-75-C-1012 b. PROJECT NO. c. d.	9b. OTHER REPORT NO(S) (Any other numbers that may be assigned this report)

10 DISTRIBUTION STATEMENT

This document is unclassified. Reproduction and distribution for any purpose of the US government is permitted.

11 SUPPLEMENTARY NOTES	12. SPONSORING MILITARY ACTIVITY
	Office of Naval Research

13 ABSTRACT

See attached

DD FORM 1 NOV 65 1473

Unclassified

Security Classification

14 KEY WORDS	LINK A		LINK B		LINK C	
	ROLE	WT	ROLE	WT	ROLE	WT
Fracture Hydrogen Embrittlement Deformation Nickel Hydrogen						

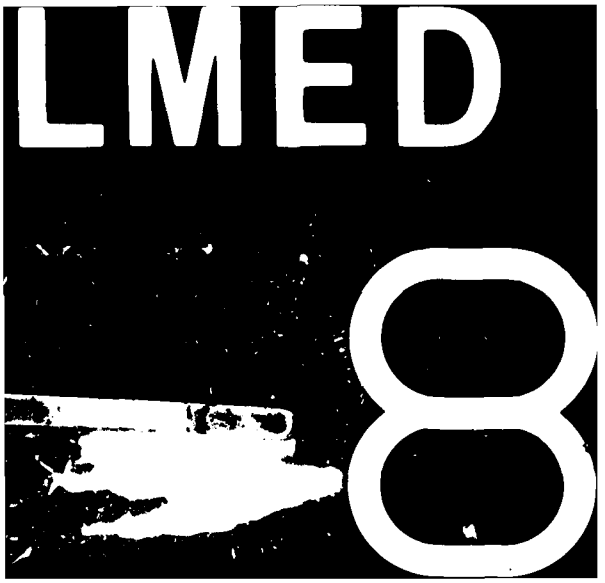
LMED
8